Analytical Calculation of No-Load Voltage Waveforms in Machines Based on Permanent-Magnet Volume Integration

Maxime R. Dubois[1] and Guillaume Mailloux[2]

[1]Department of Electrical and Computer Engineering, Université Laval, Quebec City, QC G1V 0A6, Canada
[2]Roche Canada, Rimouski, QC G5L 3A1, Canada

We develop an analytical expression for predicting electromotive force (EMF) waveforms resulting from permanent magnets (PMs) in electrical machines. The expressions for the flux linkage are based on a volume integral over the magnet volume, rather than the usual surface integral over the coil. The proposed method consists of applying a virtual current in the coil of the machine and calculating the magnetic field generated inside the PM volume. The EMF waveform is obtained by taking the derivative of the flux linkage with respect to time. We present analytical expressions of the EMF for various PM shapes and Halbach magnetization patterns. We tested a total of four configurations of PMs, and the experimental waveforms confirmed the validity of the expressions obtained theoretically.

Index Terms—**Analytical calculation, Halbach arrays, permanent-magnet machines.**

I. Introduction

FARADAY'S law states that the motion of permanent magnets (PMs) in the vicinity of a coil creates an electromotive force (EMF) across that coil. In this paper, analytical expressions will be derived for the EMF waveform. In past scientific literature, the derivation of the flux density $B_{\rm PM}$ created by the PMs is discussed, rather than the EMF or flux linkage. In [1], [3], [6], [8]–[10], $B_{\rm PM}$ is derived analytically by solving Maxwell's equation with either a scalar potential or vector potential formulation. For the EMF e, [7] proposes an expression using the space harmonics of $B_{\rm PM}$ and the stator winding factor for each harmonic, once $B_{\rm PM}$ is known.

In past literature, the PM configurations studied were usually simple (rectangular with radial or parallel magnetization of the PMs). Even with a simple magnet structure, the solutions give long analytical expressions of $B_{\rm PM}$. For more sophisticated magnet geometries, e.g., a pyramidal configuration, the complexity of the boundary conditions will give rise to significant mathematical difficulties when solving Poisson's or Laplace's equation.

In this paper, a different mathematical approach is developed for the case of more elaborate magnet geometries.

The proposed analytical method is based on the concept of volumetric flux contribution of magnet elements, developed by the author in [2]. Flux linkage is obtained by integrating the dot product of $\boldsymbol{H_a}$ (coil-created magnetic field) and $\boldsymbol{B_r}$ (PM remanent flux density) over the magnet volume, divided by the coil current i. This is useful when sophisticated magnet volumes are considered, because the magnetic field $\boldsymbol{H_a}$ is not dependent upon the magnet boundaries (for a given air-gap thickness). Finally, the electromotive force e is obtained by applying a conventional time derivative to the no-load flux linkage.

This method of PM volume integration was previously presented in [2] and is here applied to the study of the EMF in a machine with circular rotor. The case of a slotless stator core with an infinitely thin current distribution is considered in the paper and four magnet geometries are presented in order to show the usefulness of the proposed method.

II. No-Load Flux Linkage in PM Machines

A. Conventional Expression of Magnetic Flux Linkage and Faraday's Law

Faraday has described the electromotive force across a coil as the time derivative of the magnetic flux linking said coil. Usually, the magnetic flux linkage λ is calculated by integrating the flux-density over the coil surface, or mathematically

$$e = -\oint_C \vec{E}\cdot\vec{dl} = \frac{d\lambda}{dt} \tag{1}$$

where

$$\lambda = \int\int_S \vec{B}\cdot\vec{dA}\,.$$

In (1), $\boldsymbol{E}$ is the electric field, $\boldsymbol{B}$ is the magnetic flux density, and C is the contour of the coil surface S.

For the EMF of PM machines, $\boldsymbol{B}$ is the flux density generated by the PMs, considering that no current flows through the stator coil leads.

Equation (1) implies that permanent magnets are a source of magnetic flux, which is collected by the coil. The result is a flux linkage in the coil, which value depends on the source of flux density (the PMs) and the collector geometry (the coil surface), as depicted in Fig. 1.

B. Reciprocal Relationship

A mathematical expression has been developed in [2] to express the no-load flux linkage λ in a different manner

$$\lambda = \int_{V_{\rm PM}} \int\int \frac{\vec{H}_a}{i}\cdot\vec{B}_r\,dV \tag{2}$$

where λ is the flux linking in the stator coil under no-load condition, $\boldsymbol{H_a}$ is the magnetic field intensity created by the stator coil alone (that is, when the PMs are replaced by air) upon the application of a current i in the coil. $\boldsymbol{B_r}$ is the PM remanent

Digital Object Identifier 10.1109/TMAG.2008.918920

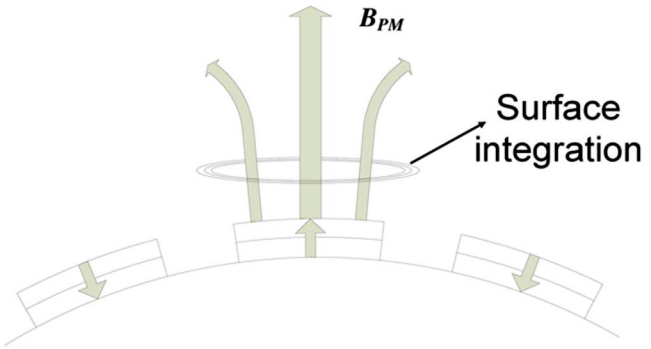

Fig. 1. The coil as a collector of B_{PM}.

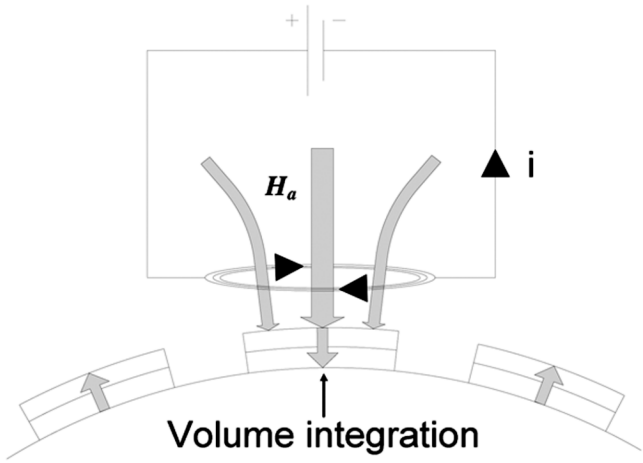

Fig. 2. The PM as a collector of H_a.

flux density and V_{PM} is the volume of the PMs. Here, we note that (2) is expressed as a volume integral of a vector operation, which is different from the conventional surface integration of (1). Equation (2) is mathematically equivalent to (1), as long as the following assumptions are met.

- — PMs have rigid magnetization, that is constant magnetization and recoil permeability $\mu_{\mathrm{recoil}} = \mu_0$.
- — Steel parts are ideal (no saturation and infinite permeability).
- — Constant magnetic vector potential throughout the coil conductors cross section, that is, assumption of filamentary conductors.

At this point, the reader may be uncomfortable with the idea that the flux linkage under no-load condition λ expressed with (2) is equivalent to (1). However, the demonstration of this equivalence was established in [2] and will not be repeated here. Experimental results presented in Section IV of the present paper will confirm the validity of (2). The mathematical form of (2) suggests that the no-load flux linkage in the coil may also be viewed as a quantity obtained when the magnetic field $\boldsymbol{H_a}$ produced by the coil is collected by the PM volume elements, each of which carries a certain remanent polarization $\boldsymbol{B_r}$.

Such expression (2) is reciprocal to the conventional expression for λ, in the sense that the source of the magnetic interaction is the coil, whereas the collector geometry is the PM volume, as depicted in Fig. 2. Provided that the mentioned assumptions are met, (2) is useful because it simplifies analytical calculations for machines with regular stator coils and irregular PM shapes.

III. No-Load Voltage for Regular and Irregular PM Shapes With an Infinitely Thin Stator Coil

In this section, an analytical expression is derived for the no-load flux linkage and electromotive force for the case of a PM machine with a simple stator winding, that is a slotless stator with an infinitely thin winding (Fig. 3). Although a simple stator winding is used, greater complexity is considered for the rotor. PMs with various block configurations are proposed [Fig. 4(b), (c), (d)]. A modification of the PM geometry will not change the analytical expression itself, but rather modify the integration boundaries, as will be discussed in Section III-C.

Four PM shapes are proposed: a simple rectangular magnet [Fig. 4(a)], a pyramidal stack [Fig. 4(b)], a T-shape magnet [Fig. 4(c)], and a Halbach array [Fig. 4(d)] with two different magnet thicknesses for the tangential and the radial magnets.

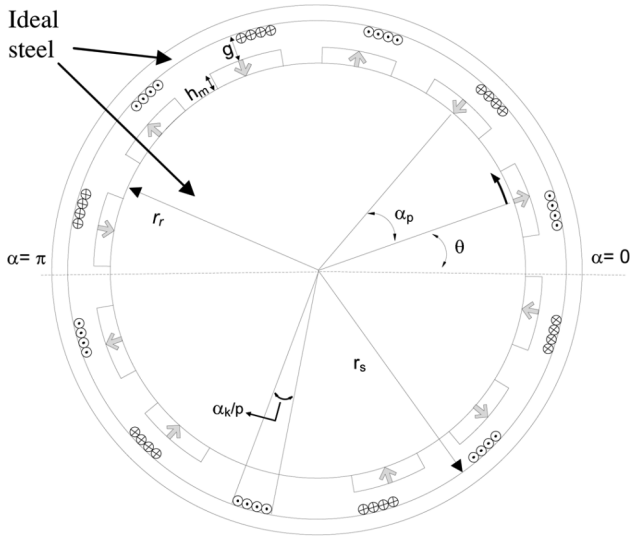

Fig. 3. The PMs in the air-gap space. Regular PM shape.

These shapes are more or less arbitrary. Other PM shapes could be analyzed with the same method.

In the analysis, r_r and r_s are respectively the radius of the rotor and the stator. h_m is the total thickness of the rotor magnets and g is the mechanical air gap. With respect to the angles presented in Fig. 3, α is the mechanical angle (in rad) with respect to the fixed stator winding (see Fig. 3). α_p is the mechanical angle occupied by one pole.

Upon rotation of the rotor, the latter will make an electrical angle θ with respect to the fixed stator (mechanical angle is θ/p). The references for $\theta = 0$ and $\alpha = 0$ are shown in Fig. 3.

The stator coil is modeled as a surface current distribution laid out on the surface of the stator laminations with constant radius r_s. The PMs are mounted on the surface of the rotor, which has a constant radius r_r.

A. Coil-Created Field

In the derivation of the no-load flux linkage λ, the first step consists in expressing the magnetic field intensity $\boldsymbol{H_a}$ created by the coil, as prescribed by (2).

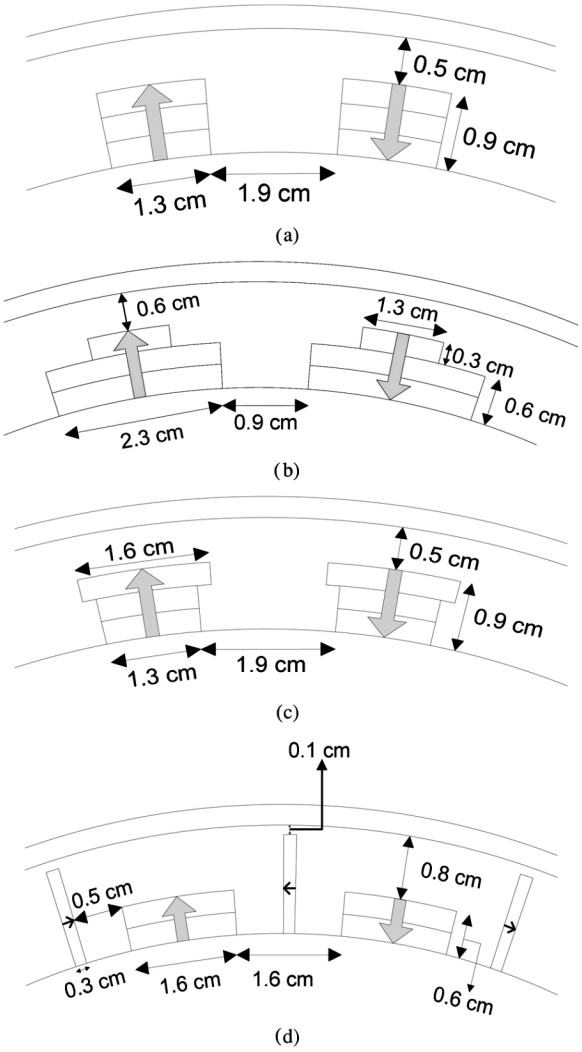

Fig. 4. Examples of regular (a) and irregular magnet geometries (b,c,d). These configurations are analyzed in the paper.

In cylindrical coordinates, the stator-created field has been derived in previous scientific literature [5] for an infinitely thin winding:

$$\frac{H_{ar}}{i} = \sum_{k=1,3,5..}^{\infty} \frac{N_k}{2r} \frac{\left(r^{2pk} + r_r^{2pk}\right)}{\left(r_s^{2pk} - r_r^{2pk}\right)} \left[\frac{r_s}{r}\right]^{pk} \cos(pk\alpha) \quad (3)$$

$$\frac{H_{a\alpha}}{i} = -\sum_{k=1,3,5..}^{\infty} \frac{N_k}{2r} \frac{\left(r^{2pk} - r_r^{2pk}\right)}{\left(r_s^{2pk} - r_r^{2pk}\right)} \left[\frac{r_s}{r}\right]^{pk} \sin(pk\alpha) \quad (4)$$

where H_{ar} and $H_{a\alpha}$ are the radial and tangential components of the stator-created magnetic field intensity in cylindrical coordinates and p is the number of pole pairs in the machine. N_k is the coil winding factor for each kth harmonic.

For example, in a full-pitch winding, N_k is expressed by

$$N_k = \frac{8N}{k\pi\alpha_k} \sin\left[\frac{\alpha_k k}{2}\right] \sin\left[\frac{\pi k}{2}\right] \quad (5)$$

where N is the total number of turns in the machine and k is the order of the harmonic [5]. α_k is the electrical angle (in rad) occupied by the coil in a full-pitch winding.

It must be noted that, in this paper, the stator winding is assumed to be symmetrical, giving only odd harmonics in (3) and (4).

B. Derivation of Electromotive Force for a Regular PM Shape

To obtain the flux linkage λ under no-load condition through one stator coil from (2), the integral volume extends from radius $r = r_r$ to radius $r = r_r + h_m$, from mechanical angle $\boldsymbol{\alpha} = -\boldsymbol{\alpha}_p/2$ to $\boldsymbol{\alpha} = +\boldsymbol{\alpha}_p/2$, and from axial length $l = 0$ to $l = l_s$. In the paper, PMs may have radial and tangential polarization components B_{rr} and $B_{r\alpha}$. For a rectangular PM shape, the tangential component $B_{r\alpha}$ is zero and the PMs are oriented radially. But with a Halbach array, the component $B_{r\alpha}$ will be considered due to the magnets oriented tangentially [see Fig. 4(d)].

As the cylindrical coordinate system is orthogonal, we may write the dot product of (2) in the following form:

$$\lambda = \int_0^{l_s} \int_{r_r}^{r_r+h_m} \int_{-\alpha_p/2}^{+\alpha_p/2} \left(\frac{H_{ar}}{i} B_{rr} + \frac{H_{a\alpha}}{i} B_{r\alpha}\right) r d\alpha dr dl. \quad (6)$$

The convention adopted for the directions of the B_r vectors are:

- the radial remanent flux density B_{rr} is positive when directed towards the stator;
- the tangential remanent flux density $B_{r\alpha}$ is positive when directed in the direction of increasing α, that is, counterclockwise.

Inserting (3) and (4) into (6), we rewrite (6) as

$$\lambda = \sum_{k=1}^{\infty} \frac{N_k}{2} \int_0^{l_s} \int_{r_r}^{r_r+h_m} \left\{ \frac{r_s^{pk}}{r^{pk}\left(r_s^{2pk} - r_r^{2pk}\right)} \cdot \left[\left(r^{2pk} + r_r^{2pk}\right) \int_{-\alpha_p/2}^{+\alpha_p/2} B_{rr}(r,\alpha)\cos(pk\alpha) d\alpha - \left(r^{2pk} - r_r^{2pk}\right) \int_{-\alpha_p/2}^{+\alpha_p/2} B_{r\alpha}(r,\alpha)\ \sin(pk\alpha) d\alpha \right] \right\} dr dl. \quad (7)$$

In (7), the PM remanent flux densities B_{rr} and $B_{r\alpha}$ are functions of the angle α and radius r, if we consider that B_r angle and value are changing around the rotor circumference. $B_{rr}(r,\alpha)$ and $B_{r\alpha}(r,\alpha)$ can be expressed as Fourier series:

$$B_{rr}(r,\alpha) = \sum_{n=1}^{\infty} \{B_{rran}(r)\cos(pn\alpha) + B_{rrbn}(r)\sin(pn\alpha)\} \quad (8)$$

$$B_{r\alpha}(r,\alpha) = \sum_{n=1}^{\infty} \{B_{r\alpha an}(r)\cos(pn\alpha) + B_{r\alpha bn}(r)\sin(pn\alpha)\}. \quad (9)$$

If the PMs are assumed as symmetrical, B_{rran} and $B_{r\alpha bn}$ are zero for all even values of n, giving

$$\lambda(\theta) = \sum_{\substack{k=1,3,5\cdots \\ n=k}}^{\infty} \frac{\pi N_k \cos(n\theta)}{4p} \int_0^{l_s} \int_{r_r}^{r_r+h_m} \left\{ \frac{r_s^{pk}}{r^{pk}(r_s^{2pk} - r_r^{2pk})} \cdots \right.$$
$$\left. \left[\left(r^{2pk} + r_r^{2pk}\right) B_{rrdn}(r) \; - \left(r^{2pk} - r_r^{2pk}\right) B_{r\alpha qn}(r) \right] \right\} dr dl. \tag{10}$$

The detailed derivation from (7) to (10) is given in the Appendix.

B_{rrdn} and $B_{r\alpha qn}$ are the space harmonic components of the PM radial remanent flux density in the d-axis and tangential remanent flux density in the q-axis. More precisely, Fig. 5(a) illustrates the convention used in (8), (9), and (10) to relate the phase and direction of B_{rrdn} (radial harmonic components of B_r) with respect to the stator winding. In a similar way, Fig. 5(b) illustrates the convention used for the phase and direction of $B_{r\alpha qn}$ (tangential harmonic components of B_r) with respect to the stator winding. Fig. 5(b) shows how the tangential magnets must be configured for a positive and maximum value of the first space harmonic of $B_{r\alpha qn}$, whereas Fig. 5(c) shows the orientation of the tangential magnets for a negative fundamental of $B_{r\alpha qn}$.

In (10), the rotor is assumed as moving with a constant speed, making an electrical angle θ with respect to the stator winding. The reference for $\theta = 0$ is taken as the rotor position for which the radial magnets face the stator winding, as shown in Fig. 5. As a convention, angle θ increases when rotor moves in the direction of increasing α.

Up to this point, all the expressions presented allowed B_r to vary with r. For greater simplicity and clarity, further derivations will assume constant values of B_r within each magnet layer. Assuming that the remanent flux density B_r is constant throughout the magnet thickness $h_m, B_{rrdn}(r)$, and $B_{r\alpha qn}(r)$ are no longer functions of r, that is $B_{rrdn}(r) = B_{rrdn}$ and $B_{r\alpha qn}(r) = B_{r\alpha qn}$. Also, we assume all fields to be two-dimensional, that is, no variable are functions of the axial length l. The double integral of (10) is solved analytically. We obtain

$$\lambda(\theta) = \frac{\pi l_s r_r}{4p} \sum_{\substack{k=1,3,5\cdots \\ n=k}}^{\infty} \frac{N_k \cos(n\theta)}{\left[1 - \left(\frac{r_r}{r_s}\right)^{pk}\right]\left[1 + \left(\frac{r_s}{r_r}\right)^{pk}\right]}$$
$$\cdot \left[\frac{\left(1 + \frac{h_m}{r_r}\right)^{1+pk} - 1}{1+pk} (B_{rrdn} - B_{r\alpha qn}) \right.$$
$$\left. + \frac{\left(1 + \frac{h_m}{r_r}\right)^{1-pk} - 1}{1-pk} (B_{rrdn} + B_{r\alpha qn}) \right] \tag{11}$$

where l_s is the axial length of the stator laminations.

It is now possible to find an expression for the EMF e, by using Faraday's law

$$e(\theta) = 2p\frac{d\lambda(\theta)}{dt} = 2p\frac{d\lambda(\theta)}{d\theta}\frac{d\theta}{dt} = \frac{4\pi p^2 \gamma}{60}\frac{d\lambda(\theta)}{d\theta} \tag{12}$$

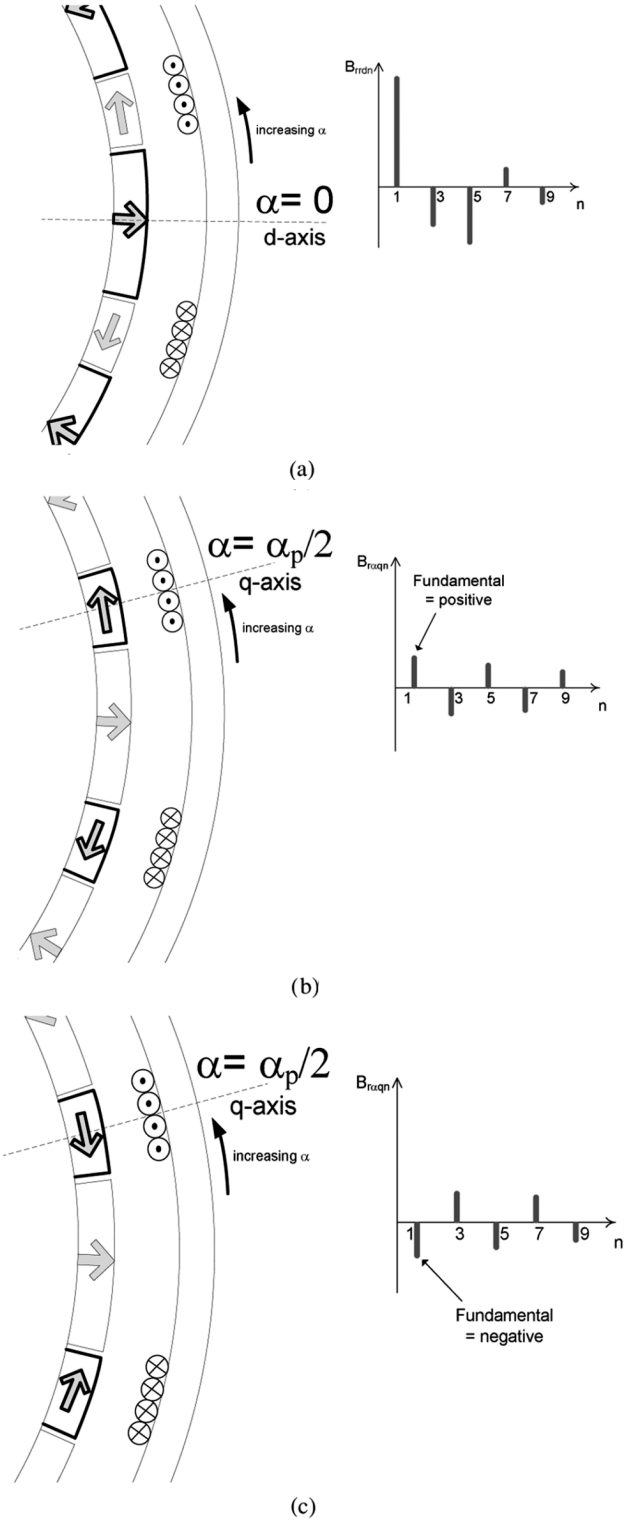

Fig. 5. Conventions for d-axis and q-axis remanent flux densities. Rotor electrical angle is $\theta = 0$. (a) $\theta = 0$, rotor position for positive and maximum B_{rrd1} (b) $\theta = 0$, tangential PM layout for positive and maximum $B_{r\alpha q1}$ (c) $\theta = 0$, tangential PM layout for negative $B_{r\alpha q1}$.

where γ is the machine rotational speed in rpm. The factor $2p$ at the beginning of (12) indicates that the EMF is calculated for all the poles in the machine.

Inserting (11) into (12), we obtain (13), which provides a direct relation between the EMF e and the space harmonics of the remanent flux density patterns $B_{rrdn}, B_{r\alpha qn}$ of the magnets

$$e(\theta) = -\frac{\pi^2 l_s r_r p\gamma}{60} \sum_{\substack{k=1,3,5\dots \\ n=k}}^{\infty} \frac{N_k n \sin(n\theta)}{\left[1-\left(\frac{r_r}{r_s}\right)^{pk}\right]\left[1+\left(\frac{r_s}{r_r}\right)^{pk}\right]} \cdot \left[\frac{\left(1+\frac{h_m}{r_r}\right)^{1+pk}-1}{1+pk}(B_{rrdn}-B_{r\alpha qn}) + \frac{\left(1+\frac{h_m}{r_r}\right)^{1-pk}-1}{1-pk}(B_{rrdn}+B_{r\alpha qn})\right]. \quad (13)$$

C. Derivation of EMF for an Irregular PM shapes

In Section III-B, we derived expressions for e and λ for a regular PM shape, i.e., rectangular magnet with a thickness of h_m laid out on the surface of the rotor. In this section, the analysis will be extended to less conventional PM shapes, consisting of two layers of magnets of different widths. In (10), the boundaries of integration were r_r and $r_r + h_m$. For the case of segmented magnets with variable widths for each segment, the integral of (10) will be expressed as a sum of two volume integrals, that is, one volume integral for each magnet layer.

The advantage of this method, based on the integral calculated over the magnet volume, is that no new analytical expression is needed. Equation (10) can be used and only the boundaries need to be changed.

Fig. 6 shows how the decomposition is made. For each magnet layer, a flux linkage (λ_1 for h_{m1} and λ_2 for h_{m2}) and an EMF (e_1 for h_{m1} and e_2 for h_{m2}) are calculated. Total flux linkage and EMF are obtained by summing the two components. When the calculation is made for one layer, we assume that the other part is equivalent to air. With this assumption, the superposition theorem can be applied. In our case, the volume has been separated in two regions, but if necessary, it could be done for several regions and the same principle could be used.

From (10), we write the flux linkage. Layer 1 goes from $r = r_r$ to $r = r_r + h_{m1}$ and part 2 goes from $r = r_r + h_{m1}$ to $r = r_r + h_m$, where h_{m1} is the height of the first segment

$$\lambda = \lambda_1 + \lambda_2 \quad (14)$$

$$\lambda_1(\theta) = \sum_{\substack{k=1,3,5\dots \\ n=k}}^{\infty} \frac{\pi N_k \cos(n\theta)}{4p} \int_0^{l_s r_r + h_{m1}} \int_{r_r} \left\{ \frac{r_s^{pk}}{r^{pk}\left(r_s^{2pk}-r_r^{2pk}\right)} \cdots \left[\left(r^{2pk}+r_r^{2pk}\right) B_{rrdn1} - \left(r^{2pk}-r_r^{2pk}\right) B_{r\alpha qn1}\right] \right\} drdl \quad (15)$$

$$\lambda_2(\theta) = \sum_{\substack{k=1,3,5\dots \\ n=k}}^{\infty} \frac{\pi N_k \cos(n\theta)}{4p} \int_0^{l_s r_r + h_m} \int_{r_{r+h_{ml}}} \left\{ \frac{r_s^{pk}}{r^{pk}\left(r_s^{2pk}-r_r^{2pk}\right)} \cdots \dots \left[\left(r^{2pk}+r_r^{2pk}\right) B_{rrdn2} - \left(r^{2pk}-r_r^{2pk}\right) B_{r\alpha qn2}\right] \right\} drdl. \quad (16)$$

Fig. 6. PM integration volume.

The space harmonics B_{rrdn} and $B_{r\alpha qn}$ are identified with indices 1 and 2, because the radial and tangential space harmonics of layer 1 are not the same as for layer 2. Equations (15) and (16) are solved as follows:

$$\lambda_1(\theta) = \frac{\pi l_s r_r}{4p} \sum_{\substack{k=1,3,5\dots \\ n=k}}^{\infty} \frac{N_k \cos(n\theta)}{\left[1-\left(\frac{r_r}{r_s}\right)^{pk}\right]\left[1+\left(\frac{r_s}{r_r}\right)^{pk}\right]} \cdot \left[\frac{(1+h_{m1}/r_r)^{1+pk}-1}{1+pk}(B_{rrdn1}-B_{r\alpha qn1}) + \frac{(1+h_{m1}/r_r)^{1-pk}-1}{1-pk}(B_{rrdn1}+B_{r\alpha qn1})\right] \quad (17)$$

$$\lambda_2(\theta) = \frac{\pi l_s r_r}{4p} \sum_{\substack{k=1,3,5\dots \\ n=k}}^{\infty} \frac{N_k \cos(n\theta)}{\left[1-\left(\frac{r_r}{r_s}\right)^{pk}\right]\left[1+\left(\frac{r_s}{r_r}\right)^{pk}\right]} \cdot \left[\frac{(1+h_m/r_r)^{1+pk}-(1+h_{m1}/r_r)^{1+pk}}{1+pk}(B_{rrdn2}-B_{r\alpha qn2}) + \frac{(1+h_m/r_r)^{1-pk}-(1+h_{m1}/r_r)^{1-pk}}{1-pk}(B_{rrdn2}+B_{r\alpha qn2})\right]. \quad (18)$$

The EMF is obtained by derivating (17) and (18) with respect to θ. We obtain

$$e(\theta) = e_1(\theta) + e_2(\theta) \quad (19)$$

where

$$e_1(\theta) = -\frac{\pi^2 l_s r_r p\gamma}{60} \sum_{\substack{k=1,3,5\dots \\ n=k}}^{\infty} \frac{N_k n \sin(n\theta)}{\left[1-\left(\frac{r_r}{r_s}\right)^{pk}\right]\left[1+\left(\frac{r_s}{r_r}\right)^{pk}\right]} \cdot \left[\frac{(1+h_{m1}/r_r)^{1+pk}-1}{1+pk}(B_{rrdn1}-B_{r\alpha qn1}) + \frac{(1+h_{m1}/r_r)^{1-pk}-1}{1-pk}(B_{rrdn1}+B_{r\alpha qn1})\right] \quad (20)$$

$$e_2(\theta) = -\frac{\pi^2 l_s r_r p\gamma}{60} \sum_{\substack{k=1,3,5\dots \\ n=k}}^{\infty} \frac{N_k n \sin(n\theta)}{\left[1-\left(\frac{r_r}{r_s}\right)^{pk}\right]\left[1+\left(\frac{r_s}{r_r}\right)^{pk}\right]} \cdot \left[\frac{(1+h_m/r_r)^{1+pk}-(1+h_{m1}/r_r)^{1+pk}}{1+pk}(B_{rrdn2}-B_{r\alpha qn2}) + \frac{(1+h_m/r_r)^{1-pk}-(1+h_{m1}/r_r)^{1-pk}}{1-pk}(B_{rrdn2}+B_{r\alpha qn2})\right]. \quad (21)$$

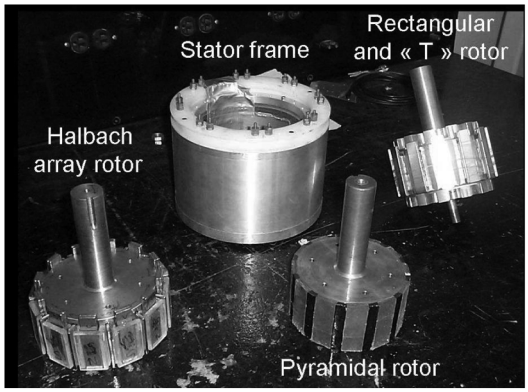

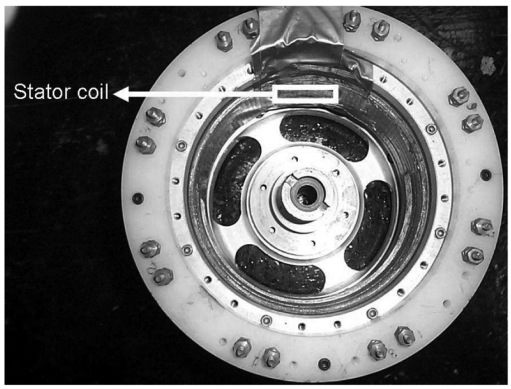

Fig. 7. Top: The three rotors used with the stator frame. Bottom: Position of the stator coil.

TABLE I
GEOMETRICAL PARAMETERS OF THE FOUR ROTOR CONFIGURATIONS

Parameters	Symbol	Rectangular	Pyramidal	"T"	Halbach	Units [a]
Pole number	2p	12	12	12	12	—
Winding	-	Full-pitch	Full-pitch	Full-pitch	Full-pitch	
Number of turns per coil	N / 2p	5	5	5	5	—
Rotor radius	r_r	0.061	0.060	0.061	0.061	m
Stator radius	r_s	0.075	0.075	0.075	0.075	m
Airgap thickness	g	5	6	5	8.2 (radial) 1.2 (tangent)	mm
Radial thickness	h_m	9	9	9	6 (radial) 13 (tangent)	mm
Magnets Electrical arc	–	73	132 (base) 73 (top)	73 (base) 90 (top)	90 (radial) 13 (tangent)	°
Coil width	α_k	2.3	2.3	2.3	2.3	°
Pole-pitch	α_p	30	30	30	30	°
Magnet remanence	B_r	1.15	1.15	1.15	1.15	T
Coil length	l_s	20	20	20	20	mm
Coil width	—	39.3	39.3	39.3	39.3	mm
Rotational speed	γ	1462	733	1355	1345	rpm

[a] m = meter, °= degrees, T = tesla, rpm = revolutions per minut e

With the last two expressions summed up, the EMF of magnet shapes with two different widths can be predicted. Four magnet shapes are presented in Section IV.

IV. EXPERIMENTAL RESULTS

In this section, four magnet geometries are illustrated:

- Rectangular-1 layer—radial magnetization;
- Pyramidal-2 layers—radial magnetization;
- T-shape-2 layers—radial magnetization;
- Halbach-2 layers—radial and tangential magnetizations.

For each configuration, the space harmonics of the remanent flux densities B_{rrdn} and $B_{r\alpha qn}$ are illustrated, with the theoretical EMF waveform calculated with (19), (20), and (21). For each configuration, a rotor and stator were built and the EMF waveform was measured with an oscilloscope across 1 coil made of five turns, as shown in Fig. 7 (bottom).

Fig. 7 illustrates the electrical machine and the rotors used in the experiments. In Fig. 7 (top), three rotors are illustrated. The four configurations could not be shown on the same picture because only three rotors were used. The T configuration was prepared with the rightmost rotor in the picture, where additional magnets were glued with a larger width than those already fixed, at the center of each pole to obtain the T. The parameters of each configuration are given in Table I. Fig. 7 (bottom) shows where the stator coil is positioned. We note that it is directly on the stator laminations and its axial length (2.0 cm) is shorter than the laminations axial length to minimize end effects. Here, PMs have an axial length of at least 5 cm. The coil width is set equal to the pole pitch, which is 3.93 cm.

The experimental EMF waveforms are illustrated in Figs. 8(c), 9(c), 10(c), and Fig. 11(c) and compared with the theoretical waveforms on the same figure. For a rectangular magnet shape with radial magnetization, Fig. 8 shows the magnet configuration, the spectral content of the remanent flux density in the radial direction B_{rrdn}, and the experimental and theoretical EMF waveforms.

The results presented in Fig. 8 indicate a good agreement between the theoretical waveform obtained with (13) and the experimental waveform.

In Figs. 9 and 10, two-layer magnet configurations are considered, with a pyramidal stack of magnets and a T configuration. The results presented in Figs. 9 and 10 indicate a good agreement between the theoretical waveforms obtained with (19), (20), (21), and the experimental waveforms.

In Fig. 11, a new characteristic is present that is not in the other figures: the tangential component. In the Halbach array of Fig. 11, both components, radial and tangential, are presented. They will both considerably affect the output of the generator. On the upper half of the PM arrangement of Fig. 11(a), only tangential PMs are present. For that upper magnet layer, the space harmonic content considered is the tangential harmonic content $B_{r\alpha n}$ only. In the upper half, the radial harmonic content is zero for all B_{rrn}.

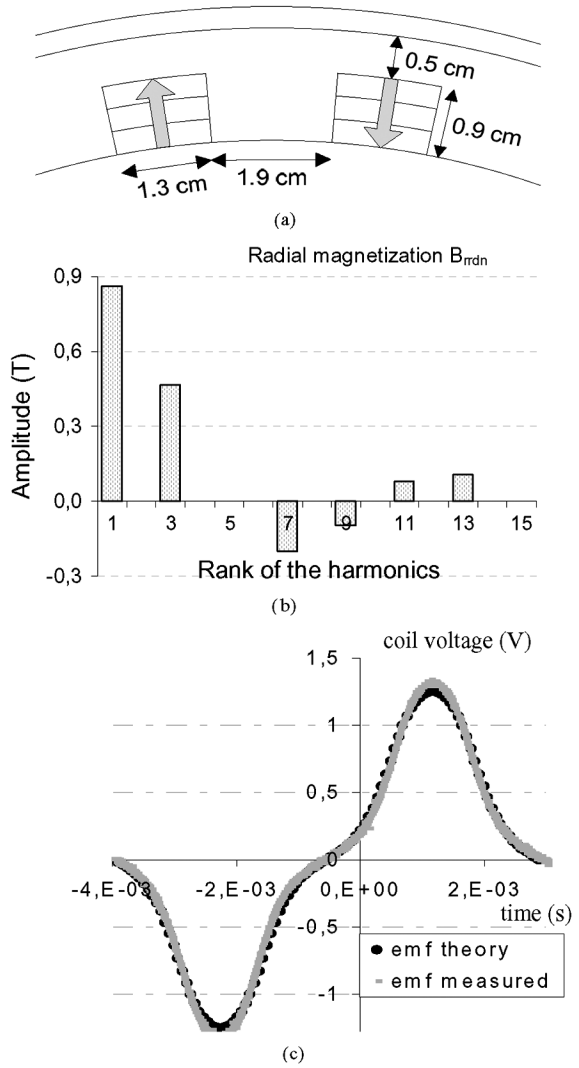

Fig. 8. Results with the rectangular shape. (a) Magnet configuration. (b) Space harmonics of the PM remanent flux density. (c) Experimental and theoretical voltage waveforms at no-load across one coil of five turns.

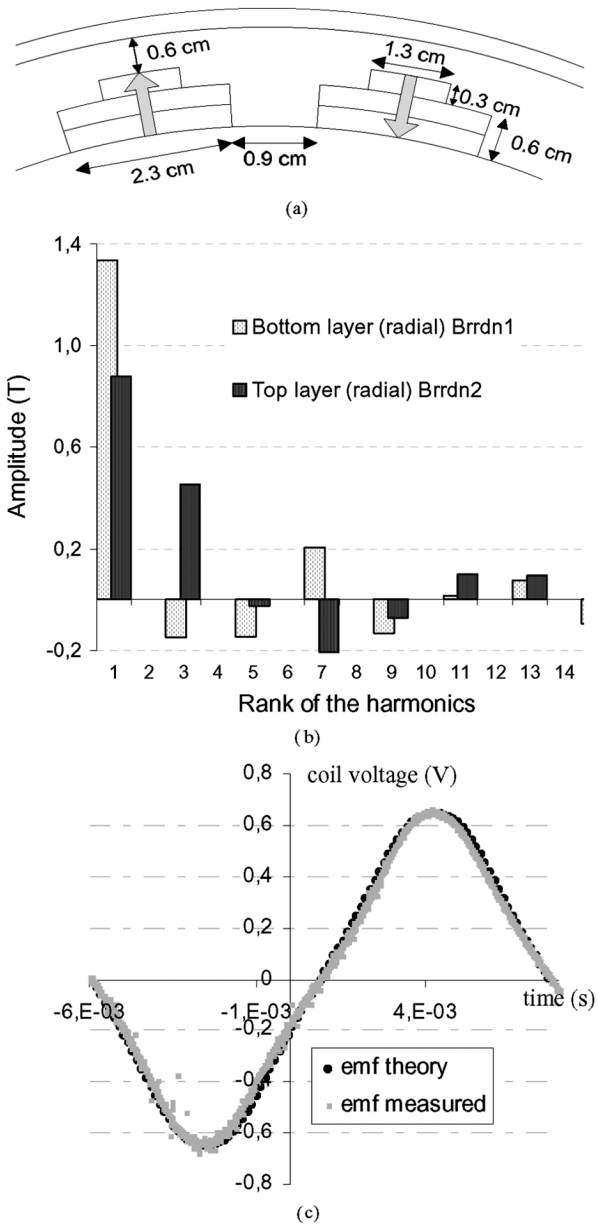

Fig. 9. Results with the pyramidal shape. (a) Magnet configuration. (b) Space harmonics of the PM remanent flux density. (c) Experimental and theoretical voltage waveforms at no-load across one coil of five turns.

It must be noted that the tangential-radial configuration proposed in Fig. 11 is probably not very useful for a true application. Nevertheless, it draws our attention, since it is a very unconventional geometry and is presented here for the sole purpose of validating the mathematical expressions derived in the paper. As a matter of fact, the results presented in Fig. 11 indicate a good agreement between the theoretical waveform obtained with (19), (20), (21), and the experimental waveform.

V. Conclusion

The paper has presented a method for deriving the no-load flux linkage and EMF in a permanent-magnet machine, by performing a volume integral on the magnets. The method was applied to a cylindrical PM machine with surface magnets, with various magnet configurations. Analytical expressions were obtained, which predict the EMF and no-load flux waveforms very accurately. The waveforms were validated experimentally on four configurations of PMs on the rotor: a rectangular magnet configuration, a pyramidal configuration, a T configuration and a two-layer Halbach array. In each case, the waveform obtained experimentally was closely matched by the theoretical waveform.

This work has been done on an internal slotless ac PM motor, but the analysis could be extended to different stator geometries with slots or irregular forms.

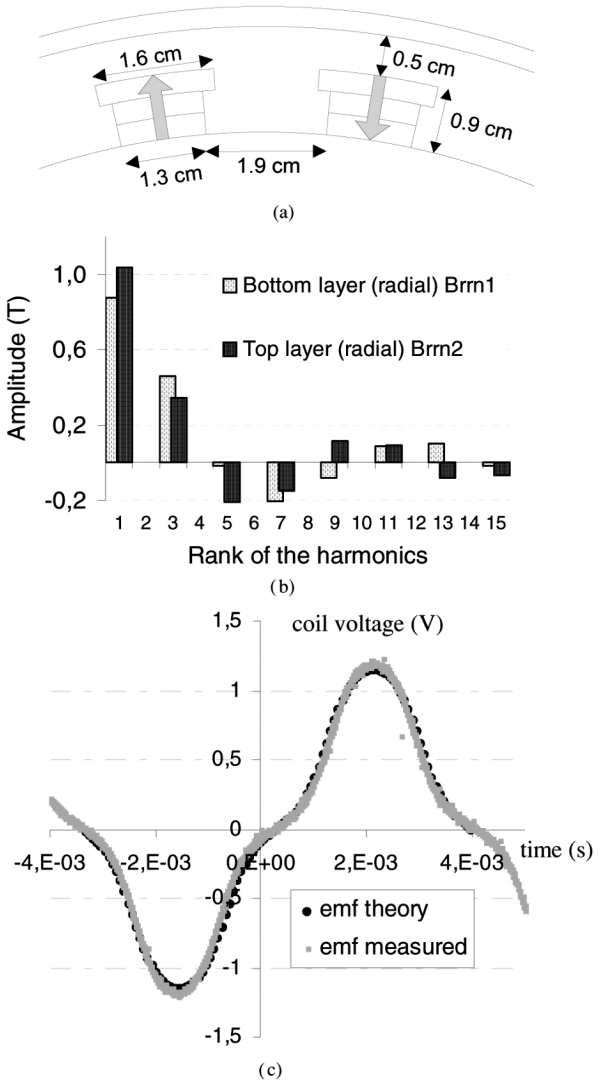

Fig. 10. Results with the "T" shape. (a) Magnet configuration. (b) Space harmonics of the PM remanent flux density. (c) Experimental and theoretical voltage waveforms at no-load across one coil of five turns.

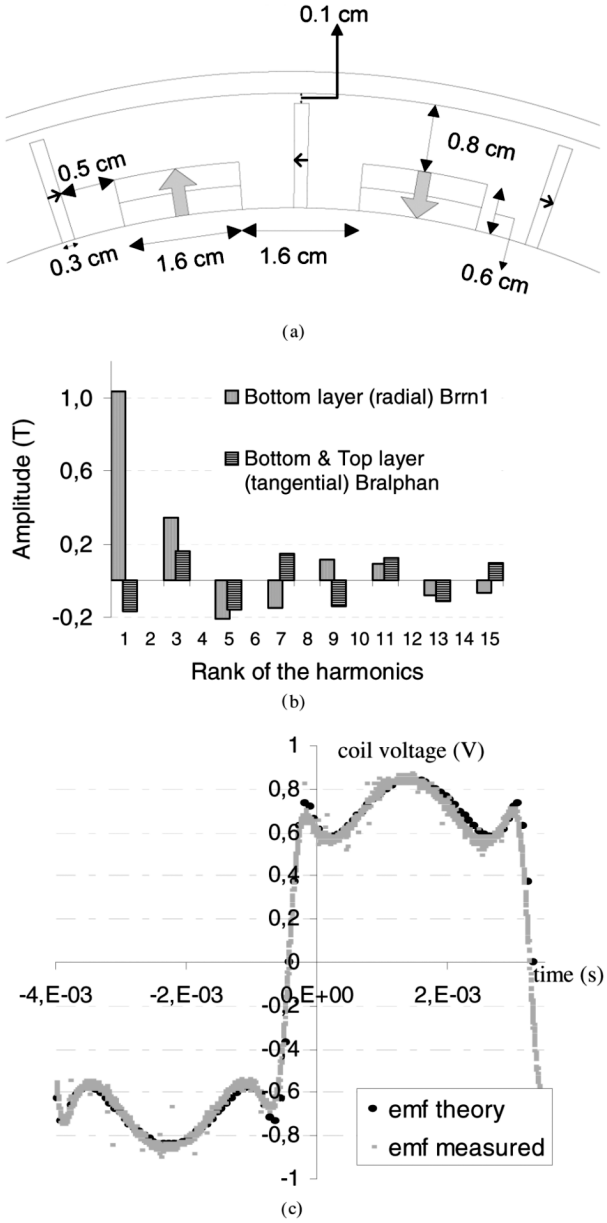

Fig. 11. Results with the Halbach array. (a) Magnet configuration. (b) Space harmonics of the PM remanent flux density. (c) Experimental and theoretical voltage waveforms at no-load across one coil of five turns.

APPENDIX

Inserting (8) and (9) into (7) leads to

$$\lambda = \sum_{k=1}^{\infty}\sum_{n=1}^{\infty}\int_0^{l_s}\int_{r_r}^{r_r+h_m}\int_{-\alpha_p/2}^{+\alpha_p/2}\frac{N_k}{2}\left\{\frac{r_s^{pk}\left(r^{2pk}+r_r^{2pk}\right)}{r^{pk}\left(r_s^{2pk}-r_r^{2pk}\right)}\right.$$
$$\cdot[B_{rran}(r)\cos(pn\alpha)\cos(pk\alpha)$$
$$+B_{rrbn}(r)\sin(pn\alpha)\cos(pk\alpha)]$$
$$-\frac{r_s^{pk}\left(r^{2pk}-r_r^{2pk}\right)}{r^{pk}\left(r_s^{2pk}-r_r^{2pk}\right)}$$
$$\cdot[B_{r\alpha an}(r)\cos(pn\alpha)\cos(pk\alpha)$$
$$\left.+B_{r\alpha bn}(r)\sin(pn\alpha)\cos(pk\alpha)]\right\}d\alpha dr dl. \quad \text{(AII.1)}$$

The four integrals of (AII.1) are solved in the α -domain as follows:

$$\int_{-\alpha_p/2}^{+\alpha_p/2}\cos(pn\alpha)\cos(pk\alpha)d\alpha$$
$$=\begin{cases}\frac{\pi}{2p} & n=k\\ 0 & n+k=\text{even}\\ \frac{1}{p}\left[\frac{\sin(n-k)\pi/2}{n-k}+\frac{\sin(n+k)\pi/2}{n+k}\right] & n+k=\text{odd}\end{cases} \quad \text{(AII.2)}$$

$$\int_{-\alpha_p/2}^{+\alpha_p/2}\sin(pn\alpha)\cos(pk\alpha)d\alpha=0 \quad \text{(AII.3)}$$

$$\int_{-\alpha_p/2}^{+\alpha_p/2}\cos(pn\alpha)\sin(pk\alpha)d\alpha=0 \quad \text{(AII.4)}$$

$$\int_{-\alpha_p/2}^{+\alpha_p/2} \sin(pn\alpha)\sin(pk\alpha)d\alpha = \begin{cases} \frac{\pi}{2p} & n=k \\ 0 & n+k=\text{even} \\ \frac{1}{p}\left[\frac{\sin(n-k)\pi/2}{n-k} - \frac{\sin(n+k)\pi/2}{n+k}\right] & n+k=\text{odd}. \end{cases} \quad \text{(AII.5)}$$

Inserting these four results in (AII.1) leads to

$$\lambda = \sum_{k=1}^{\infty}\int_0^{l_s}\int_{r_r}^{r_r+h_m}\int_{-\alpha_p/2}^{+\alpha_p/2}\frac{N_k}{2}\left\{\frac{r_s^{pk}\left(r^{2pk}+r_r^{2pk}\right)}{r^{pk}\left(r_s^{2pk}-r_r^{2pk}\right)}\cdot\left[\underbrace{B_{rran}(r)}_{n=k}\frac{\pi}{2p}+\sum_{\substack{n=1\\ n+k=\text{odd}}}^{\infty}B_{rran}(r)\frac{1}{p}\times\left[\frac{\sin(n+k)\pi/2}{n+k}+\frac{\sin(n-k)\pi/2}{n-k}\right]\right]+\frac{r_s^{pk}\left(r^{2pk}-r_r^{2pk}\right)}{r^{pk}\left(r_s^{2pk}-r_r^{2pk}\right)}\cdot\left[\underbrace{B_{r\alpha bn}(r)}_{n=k}\frac{\pi}{2p}+\sum_{\substack{n=1\\ n+k=\text{odd}}}^{\infty}B_{r\alpha bn}(r)\frac{1}{p}\times\left[\frac{\sin(n+k)\pi/2}{n+k}-\frac{\sin(n-k)\pi/2}{n-k}\right]\right]\right\}d\alpha dr dl. \quad \text{(AII.6)}$$

Assuming the winding and the magnets to be symmetrical, that is all poles have an identical winding distribution, with alternating polarities. In the same way, all rotor poles are identical, with alternating polarities. Whence, all $B_{rran}(r)$ and $B_{r\alpha bn}(r)$ are equal to 0 for $n=$ even, and all $N_k=0$ for $k=$ even. Since the condition $n+k=$ odd in (AII.6) implies that either n or k be even (because the sum of two odd numbers give an even number), the products of N_kB_{rrbn} and $N_kB_{r\alpha an}$ are equal to 0 for $n+k=$ odd. Whence (AII.6) can be rewritten as follows:

$$\lambda = \frac{\pi}{4p}\sum_{k=1,3,5\ldots}^{\infty}N_k\int_0^{l_s}\int_{r_r}^{r_r+h_m}\left\{\frac{r_s^{pk}}{r^{pk}(r_s^{2pk}-r_r^{2pk})}\cdots\left[\left(r^{2pk}+r_r^{2pk}\right)\underbrace{B_{rran}(r)}_{n=k}-\left(r^{2pk}-r_r^{2pk}\right)\underbrace{B_{r\alpha bn}(r)}_{n=k}\right]\right\}dr dl. \quad \text{(AII.7)}$$

The next step consists in expressing the components B_{rran}, and $B_{r\alpha bn}$ for arbitrary PM positions of angle θ :

$$B_{rran}(r) = B_{rrdn}(r)\cos(n\theta) \quad \text{(AII.8)}$$

$$B_{r\alpha bn}(r) = B_{r\alpha qn}(r)\cos(n\theta). \quad \text{(AII.9)}$$

If the electrical angle $\theta=0$ corresponds to the d-axis position of the rotor as shown in Fig. 5, B_{rrdn} is the space harmonic distribution of the radial remanent flux density of the PM in the d-axis. $B_{r\alpha qn}$ is the space harmonic distribution of the tangential remanent flux density of the PM in the q-axis. Inserting (AII.8) and (AII.9) into (AII.7), we obtain

$$\lambda(\theta) = \sum_{\substack{k=1,3,5\ldots\\ n=k}}^{\infty}\frac{\pi N_k\cos(n\theta)}{4p}\int_0^{l_s}\int_{r_r}^{r_r+h_m}\left\{\frac{r_s^{pk}}{r^{pk}\left(r_s^{2pk}-r_r^{2pk}\right)}\cdots\left[\left(r^{2pk}+r_r^{2pk}\right)B_{rrdn}(r)-\left(r^{2pk}-r_r^{2pk}\right)B_{r\alpha qn}(r)\right]\right\}dr dl. \quad \text{(AII.10)}$$

REFERENCES

[1] Z. Q. Zhu, D. Howe, and B. Ackermann, "Instantaneous magnetic field distribution in brushless permanent magnet dc motors I: Open-circuit field," *IEEE Trans. Magn.*, vol. 29, no. 1, pp. 124–135, Jan. 1993.

[2] M. R. Dubois, H. Polinder, and J. A. Ferreira, "Contribution of permanent magnet volume elements to the no-load voltage in machines," *IEEE Trans. Magn.*, vol. 36, no. 3, pp. 1784–1792, May 2003.

[3] Z. Q. Zhu, D. Howe, and C. C. Chan, "Improved analytical model for predicting the magnetic field distribution in brushless permanent-magnet machines," *IEEE Trans. Magn.*, vol. 38, no. 1, pp. 229–238, Jan. 2002.

[4] J. Ofori-Tenkorang and J. H. Lang, "A comparative analysis of torque production in Halbach and conventional surface-mounted permanent-magnet synchronous motors," in *Proc. IEEE IAS Annu. General Meeting*, Orlando, FL, Oct. 1995, pp. 657–663.

[5] H. Polinder, "On the losses in a high-speed permanent-magnet generator with rectifier," Ph.D. dissertation, Delft Univ. Tech., Delft, The Netherlands, 1998.

[6] N. Boules, "Two-dimensional field analysis of cylindrical machines with permanent magnet excitation," *IEEE Trans. Ind. Appl.*, vol. IA-20, no. 5, pp. 1267–1277, Sep./Oct. 1984.

[7] J. De La Ree and N. Boules, "Induced voltage harmonic reduction of PM cylindrical machines," *IEEE Trans. Ind. Appl.*, vol. 28, no. 3, pp. 619–624, May/Jun. 1992.

[8] J. De La Ree and N. Boules, "Magnet shaping to reduce induced voltage harmonics in PM machines with surface mounted magnets," *IEEE Trans. Energy Convers.*, vol. 6, no. 1, pp. 155–161, Mar. 1991.

[9] K. Halbach, "Design of permanent multipole magnets with oriented rare earth cobalt material," *Nucl. Instrum. Methods*, vol. 169, pp. 1–10, 1980.

[10] K. F. Rasmussen, J. H. Davies, T. J. E. Miller, M. I. McGilp, and M. Olaru, "Analytical and numerical computation of air-gap magnetic fields in brushless motors with surface permanent magnets," *IEEE Trans. Ind. Appl.*, vol. 36, pp. 1547–1554, Nov./Dec. 2000.

Manuscript received October 1, 2007; revised February 11, 2008. Corresponding author: M. R. Dubois (e-mail: mrdubois@gel.ulaval.ca).

Maxime R. Dubois (M'99) was born in Alma, Québec, Canada, in 1968. He received the B.Ing. and M.Sc. degrees in electrical engineering from the Université Laval, Québec, Canada, in 1991 and 1993, respectively, and the Ph.D. degree *cum laude* from Delft University of Technology, Delft, The Netherlands, in 2004.

Between 1993 and 1999, he worked as a design engineer for private companies in Canada, in the area of power electronics. Since 2004, he has been an Assistant Professor at Université Laval, in the LEEPCI laboratory. His main interests are machines and power electronics applied to the generation of energy from renewable sources.

Guillaume Mailloux was born in Rivière-du-Loup, Québec, Canada, in 1983. He received the B.Ing. degree in electrical engineering from the Université Laval, Québec, Canada, in 2007.

He is working at Roche Canada, an engineering consultant in Rimouski, Canada.